Flux Synthesis of MgNi$_2$Bi$_4$ and Its Structural Relationship to NiBi$_3$

Mary B. Hertz, Ryan E. Baumbach, and Susan E. Latturner*

ACCESS | Metrics & More | Article Recommendations | Supporting Information

ABSTRACT: MgNi$_2$Bi$_4$ was grown from the reaction of magnesium and nickel in excess bismuth flux. It forms as large, malleable crystals with a new structure type in orthorhombic space group *Cmcm*. The structure contains a building block common to Ni–Bi binary phases—nickel zigzag chains running along one direction and surrounded by bismuth. Magnetic susceptibility and transport measurements indicate that the compound is metallic; this is supported by calculations of density of states. Crystal orbital Hamilton population analyses indicate that Ni–Bi interactions are the strongest bonding interactions in the structure, whereas Bi–Bi bonding between the layers is negligible, making MgNi$_2$Bi$_4$ a potential two-dimensional material.
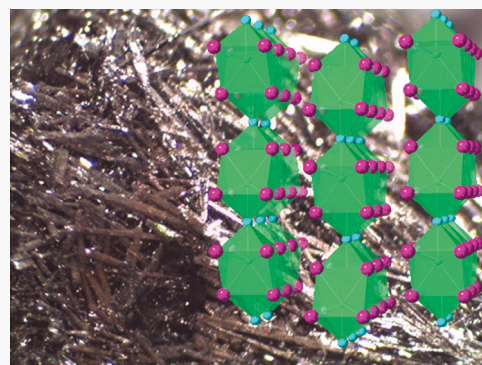
INTRODUCTION

Since the discovery of graphene,[1] there has been an increased interest in the properties of two-dimensional (2D) materials.[2,3] Such materials have surprised many with their unusual electronic and magnetic properties that range from super-conductivity[4] to high electron mobilities.[5] Isolating the 2D properties from those of the bulk material can be nontrivial as the bulk material will often require exfoliation. Structures that lend themselves to exfoliation are being pursued with great interest for applications ranging from wide band gap semiconductors to batteries to electrochromics, exemplified by reports on compounds such as MnPS$_3$, FeOCl, and MoO$_3$, as well as the extensive work on intermetallic MAX phases which can be etched to isolate their 2D transition-metal boride or carbide layers.[6−10]

Metal flux reactions have been shown to be productive for the exploratory synthesis of multinary intermetallics.[11] Flux synthesis utilizes a low melting metal, or mixture of metals, in large excess which acts as a solvent for the other species in the reaction. The use of a molten flux mediates some of the drawbacks of conventional solid-state synthesis such as diffusion barriers and associated long reaction times, repeated heating cycles, and high temperatures. The faster reactions and lower heating temperatures compared to conventional solid-state reactions allow for formation of kinetic products rather than the thermodynamic phases favored by high temperatures. Additionally, because flux synthesis is a solution-based method, slow cooling of the melt can lead to crystal growth. Bismuth metal is attractive as a flux given its low melting point (271 °C) and ability to dissolve a wide range of elements; this is demonstrated by the crystallization of LaCo$_2$As$_2$ and RERh$_6$P$_4$ (RE = Sc, Yb, Lu) from Bi melts.[12,13]

In this work, reactions of magnesium and nickel in bismuth flux were explored, yielding large crystals of the new ternary intermetallic phase MgNi$_2$Bi$_4$. Bismuth-rich intermetallics are of great interest in solid-state chemistry/condensed-matter physics research. Bismuth can exhibit large diamagnetism, strong spin–orbit coupling, and relativistic effects which contribute to exotic behaviors in bismuth compounds such as quantum spin Hall effects (bismuth thin films), topological phenomena (Na$_3$Bi, Bi$_2$Te$_3$), and superconductivity (NiBi$_3$).[14,15] The title compound MgNi$_2$Bi$_4$ forms with a new structure type that contains Ni/Bi building blocks similar to those found in binary Ni–Bi phases including the superconducting NiBi$_3$. The Ni–Bi system has previously been investigated at both ambient and high pressures; the binary phases show a range of dimensionality from quasi-1D NiBi$_3$, quasi-2D NiBi$_2$, and 3D β-NiBi.[16] Electronic structure calculations for MgNi$_2$Bi$_4$ indicate that the compound is metallic and that the nickel–bismuth bonding interactions are crucial to stabilizing the material and may result in low dimensional behavior.

EXPERIMENTAL PROCEDURE

Synthesis. Bismuth granules (99.997%, Alfa Aesar), nickel powder (99.8%, Alfa Aesar), and magnesium granules (99.8%, Alfa Aesar) were combined in a 10:2:1 mmol ratio in an alumina crucible. This crucible was placed in a silica tube and topped with a piece of quartz wool; the tube was then flame-sealed under vacuum. The ampule was

heated to 800 °C over 12 h, maintained at 800 °C for 30 h, cooled to 500 °C over 36 h, held at 500 °C for 24 h, and finally cooled to 350 °C over 30 h. At this temperature, it was removed from the furnace, inverted, and centrifuged in order to strip excess molten flux away from the crystallized products.

Elemental Analysis. Products were analyzed using energy dispersive spectroscopy (SEM-EDS) with a FEI Nova 400 NanoSEM scanning electron microscope. Because of the lamellar nature of $MgNi_2Bi_4$, layers of this material can be peeled off, making it easy to obtain very thin layers of the crystal. In order to analyze the interior of the material, crystals were adhered to a piece of double-sided carbon tape and then lifted back off, leaving behind a thin layer with a surface clear of flux residue. In addition to determining Mg/Ni/Bi ratios, we also screened samples for possible incorporation of aluminum from the crucible. EDS of crystals from a variety of synthesis batches indicated an average atomic composition of 15.4(9)% Mg, 25.1(3)% Ni, and 59.0(5)% Bi. EDS analysis in the absence of calibration standard samples is known to be semiquantitative, but the observed ratio supports the results of single-crystal XRD data.

Crystallographic Studies. Crystallographic data were collected using both single-crystal and powder X-ray diffraction techniques. Single-crystal XRD data were collected at room temperature on a Bruker SMART APEX2 CCD diffractometer with a Mo Kα X-ray tube (λ = 0.71073 Å). Because of the malleable nature of the $MgNi_2Bi_4$ crystals, it was necessary to select a sufficiently small crystal (size $1.0 \times 0.08 \times 0.08$ mm^3) rather than cleaving a piece from a larger crystal to avoid introducing defects. The crystal was mounted using paratone oil on a cryoloop. The data were integrated using the SAINT program,[17] and an absorption correction was applied with the SADABS program.[18] The structure was then solved using direct methods with the SHELX software[19] in order to locate the bismuth and nickel atoms, followed by a combined use of least-squares refinement and Fourier difference maps in order to place the lighter magnesium atoms. Thermal parameters were refined anisotropically for all atoms. Details of crystallographic data collection and refinement are found in Table 1. Atomic positions and thermal parameters are given in Table S1 of the Supporting Information; additional data (available as a CIF file) are available from the Cambridge Structural Database under file number 1961839.

In order to collect powder XRD patterns, the large crystals were ground into powder. Due to the malleability of $MgNi_2Bi_4$, simple mortar and pestle grinding smeared the solids rather than fracturing the crystals into a powder form. A cryogenic grinding process was therefore used in hopes of making the crystals brittle and more easily fractured. $MgNi_2Bi_4$ crystals were put into acetone in a 1 dram vial, which was then placed into a container of dry ice along with an agate mortar and pestle. Once the contents of the vial reached a temperature of, at most, −70 °C, the mixture was transferred into the mortar and quickly ground into a slurry. After it warmed to room temperature, the acetone evaporated, and a polycrystalline powder was obtained. In order to further minimize the contributions of preferred orientation, the powder was put on a bed of petroleum jelly (Aquaphor) so that random orientations were encouraged and held in suspension. Powder XRD data were collected on a Panalytical 'Xpert Pro MPD, using a copper source and an X'Celerator RTMS detector, and can be found in the Supporting Information (Figure S1).

Electronic Calculations. Electronic structure calculations of band structure, density of states (DOS), and crystal orbital Hamilton population (COHP) were carried out using the Stuttgart TB-LMTO-ASA program.[20−23] Calculations were based on the atomic positions determined from the single-crystal XRD refinement. The κ-mesh was set to $24 \times 24 \times 8$. The basis sets used were: Mg (3s, 3p), Ni (4s, 4p, 3d), Bi (6s, 6p) with Mg (3d), Ni (4f), and Bi (6d, 5f) being downfolded. Empty spheres were needed for the calculation (1s).

Resistivity and Magnetic Measurements. Magnetic susceptibility and magnetization measurements were carried out for coaligned bundles of single crystal specimens (total mass 28.4 mg) at temperatures of T = 1.8−300 K under an applied magnetic field of H = 5 kOe and at T = 1.8 K for H < 7 T using a Quantum Design VSM magnetic property measurement system. The field was applied both parallel and perpendicular to the long axis of the crystals. The samples were embedded in GE-varnish and attached to a quartz rod for the measurement. The electrical resistivity ρ was measured in a four-wire configuration for temperatures of T = 1.8−300 K for current along the needle axis (measurements perpendicular to this axis were not possible due to the small width of the crystal) using a Quantum Design physical property measurement system.

RESULTS AND DISCUSSION

Synthesis. $MgNi_2Bi_4$ forms as silver rod-like crystals up to 5 mm in length and 0.25 mm in width. Most crystals are clean of visible flux and grow as clusters (see Figure 1). Attempts to manipulate and physically separate crystals from one another revealed that the crystals are very malleable. As such, most measurements requiring a single crystal, notably SC-XRD, required extensive searching through the product matrix for a suitable sample and extremely careful handling of the crystal so as not to bend it, creating dislocations and other defects. Flux residue on the surface of the crystals cannot be manually removed since this would cause the crystals to deform. Large crystals cannot be cut down into smaller, cleaner pieces, since this causes the crystal to splay out into sheets with curled edges. Crystals of $MgNi_2Bi_4$ are air stable for several months, and the powder is air stable for at least 2 weeks. Elemental analysis and powder XRD studies of the reaction product mixture indicates that it contains mostly $MgNi_2Bi_4$, with typically less than 5% of both $NiBi_3$ and residual bismuth flux. Elemental analysis by EDS largely agreed with the $MgNi_2Bi_4$ formula, although some crystals did show very small streaks of aluminum-rich areas. These streaks are likely a result of impurity accumulation along dislocation defects in the crystals (see Figure S2).[24] It is likely that aluminum is leached from the alumina crucible due to the presence of the strongly reducing magnesium metal reactant. The presence of aluminum is not necessary for the formation of this phase, as $MgNi_2Bi_4$ crystals can also be grown from flux reactions in stainless steel crucibles.

Table 1. Crystallographic Data Collection Parameters for $MgNi_2Bi_4$

formula weight (g/mol)	977.65
crystal system	orthorhombic
space group	Cmcm (#63)
a (Å)	4.023(2)
b (Å)	13.396(7)
c (Å)	12.593(7)
Z	4
volume (Å^3)	678.6(6)
density, calcd (g/cm^3)	9.569
radiation	Mo Kα (λ = 0.71073 Å)
temperature (K)	173
index ranges	$-5 \leq h \leq 5$, $-17 \leq k \leq 17$, $-16 \leq l \leq 16$
reflections collected	3610
unique data/parameters	502/24
μ (mm^{-1})	108.59
R_1/wR_2[a]	0.0300/0.0772
R_1/wR_2 (all data)	0.0321/0.0794
largest peak/hole	2.835/−3.000
GoF	0.885

[a] $R_1 = \Sigma(|F_0| - |F_c|)/\Sigma|F_0|$; wR_2

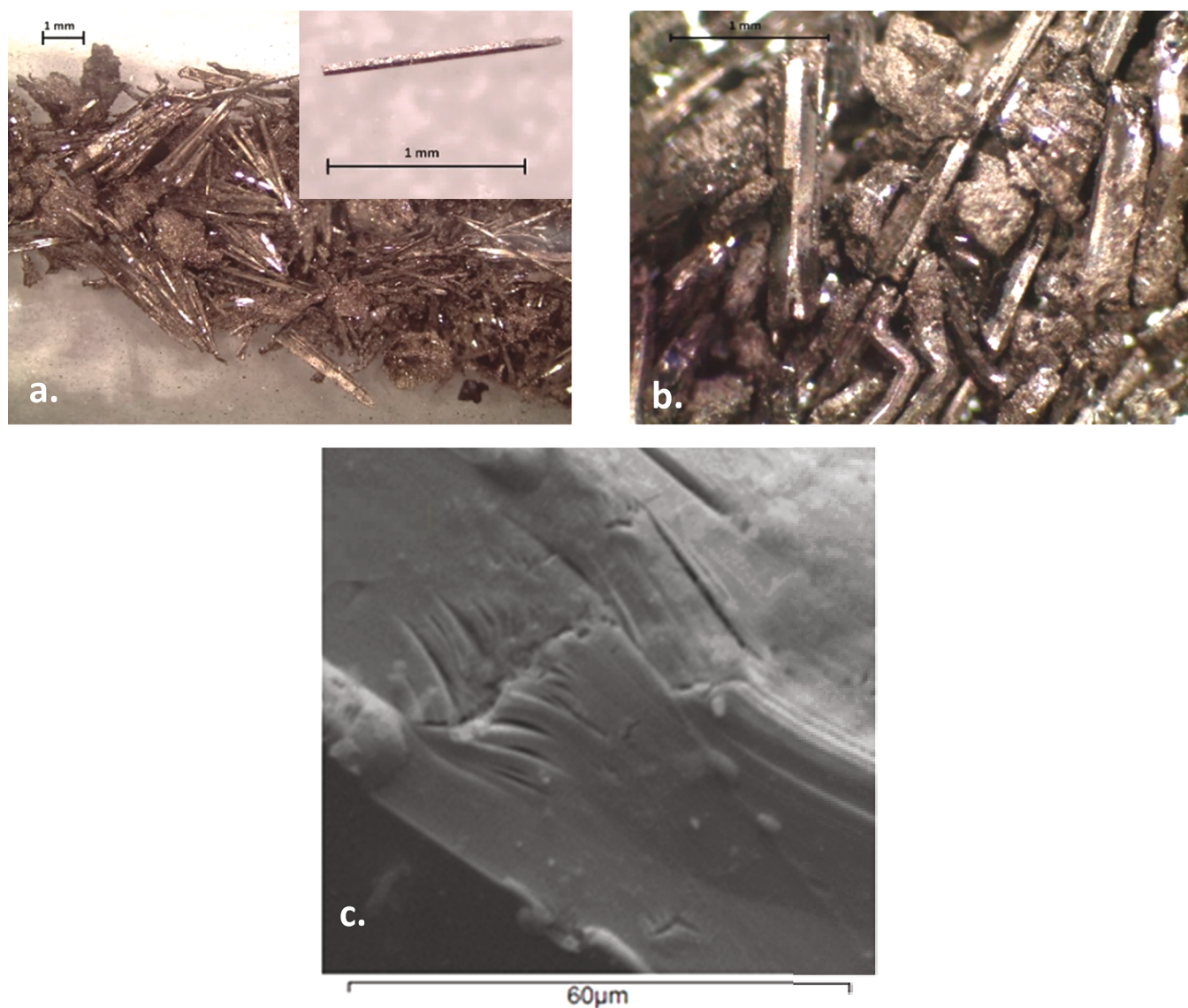$$= [\Sigma[w(F_0{}^2 - F_c{}^2)^2]/\Sigma(w|F_0|^2)^2]^{1/2}$$

Figure 1. MgNi$_2$Bi$_4$ crystals grown from bismuth flux. (a) Optical microscope image of clusters of needle-like crystals. (b) Optical microscope image showing 90° bending deformation of crystal. (c) SEM image of crystal, showing splaying of sheets that occurs upon manipulation.
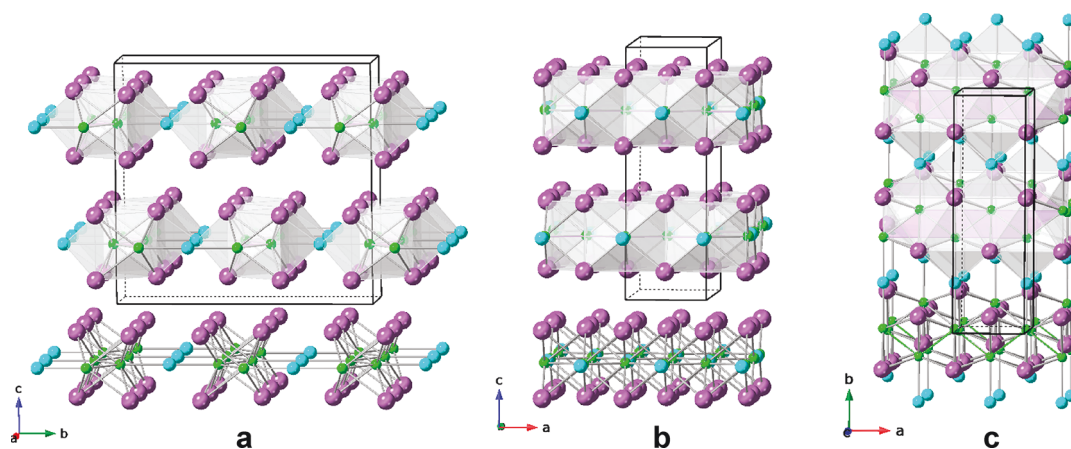

Figure 2. Crystal structure of MgNi$_2$Bi$_4$ shown in partial polyhedral mode to highlight coordination around nickel atoms. Bi atoms are purple spheres, Mg atoms are blue, and Ni atoms are green/inside gray polyhedra. (a) Structure viewed along a-axis. (b) Structure viewed along b-axis. (c) Structure viewed along c-axis.
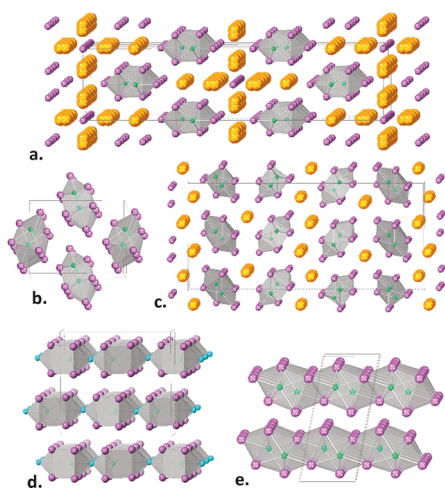
Figure 3. Bismuth/nickel binary and ternary phases; bismuth-encapsulated nickel chains are shown as gray polyhedra, and iodine is indicated by yellow spheres. (a) $Ni_4Bi_{12.86}I_6$, (b) $NiBi_3$, and (c) $Ni_4Bi_{12}I_3$ demonstrate pseudo-1D morphology of bismuth-encapsulated nickel zigzag chains, whereas (d) $MgNi_2Bi_4$ and (e) $NiBi_2$ illustrate 2D morphology of the same chain units.

Structure. $MgNi_2Bi_4$ crystallizes in a new structure type in orthorhombic space group $Cmcm$ (see Figure 2). All atom positions in $MgNi_2Bi_4$ are fully occupied, with no site mixing. The structure features zigzag chains of nickel running in the a-axis direction, linked to adjacent chains through a magnesium atom. Each nickel atom is further coordinated by bismuth atoms to form a trigonal prism monocapped with magnesium. Nickel zigzag chains encapsulated by bismuth are featured in several other binary and ternary phases, including the superconductor $NiBi_3$, the recently discovered high pressure phases $NiBi_2$ and β-$NiBi$, and the subhalide compounds $Ni_4Bi_{12}I_3$ and $Ni_4Bi_{12.86}I_6$ (see Figure 3).[16,25−27] These structures are differentiated by the positioning and linkages between these 1-D chain units. In $NiBi_3$, the encapsulated chains are separated; they are stacked in a herringbone fashion and are linked through weak Bi−Bi interactions (Bi−Bi bonds not drawn in Figure 3b). Application of high pressure yields $NiBi_2$ and β-$NiBi$, which have the chains bridged through
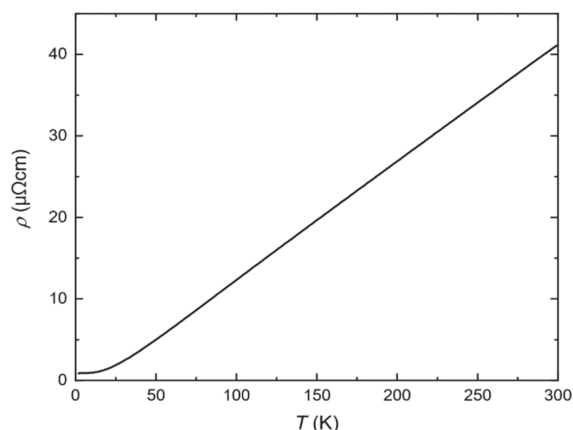

Figure 5. Temperature dependence of resistivity along the a-axis of a single crystal of $MgNi_2Bi_4$.

increasing numbers of shared bismuth vertices. Conversely, the bismuth-encapsulated nickel chains are further separated from each other by iodide building blocks in the ternary subhalide compounds.

Comparison of the bond lengths in these encapsulated chains reveal some trends. The Ni−Ni bond distance in the zigzag chain is above 2.60 Å in the binary phases $NiBi_2$ and $NiBi_3$ (2.608 and 2.633 Å, respectively). It is shorter in the ternary phases. The subiodides $Bi_{12}Ni_4I_3$ and $Bi_{12.86}Ni_4I_6$ have Ni−Ni bond lengths of 2.550 and 2.518 Å, respectively; this was postulated to be due to the effective "oxidation" of the parent $NiBi_3$ by the incorporation of iodine.[26] However, incorporation of magnesium (which could be viewed as a "reduction") also shortens the Ni−Ni bond length to 2.537(2) Å. On the other hand, the Ni−Bi bond lengths in all of these compounds lie within a similar range. $MgNi_2Bi_4$ has Ni−Bi bond lengths between 2.722(1)−2.833(2) Å, which is in good agreement with the corresponding bonds in the $NiBi_2$ structure which range from 2.721 to 2.9194 Å. These bonds in $NiBi_3$ and $Bi_{12}Ni_4I_3$ also fall within this range. This suggests that the Ni−Bi interactions are somewhat independent of the changes in the other parts of the structure and may be the key stabilizing element in this family of compounds.
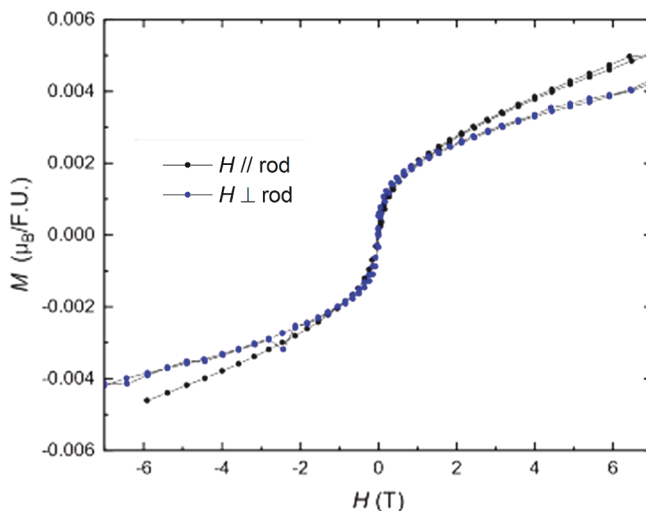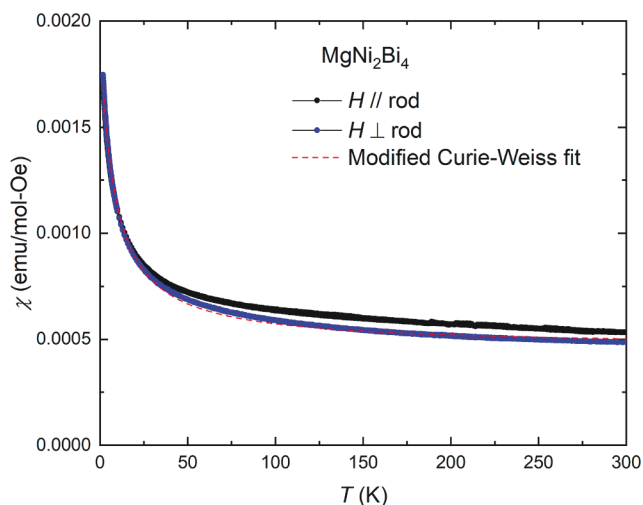

Figure 4. Magnetic susceptibility data for coaligned crystals of $MgNi_2Bi_4$ with a-axes aligned parallel or perpendicular to the field. (a) Temperature dependence of the susceptibility in an applied field of 5 kOe. (b) Magnetization data collected at 1.8 K.
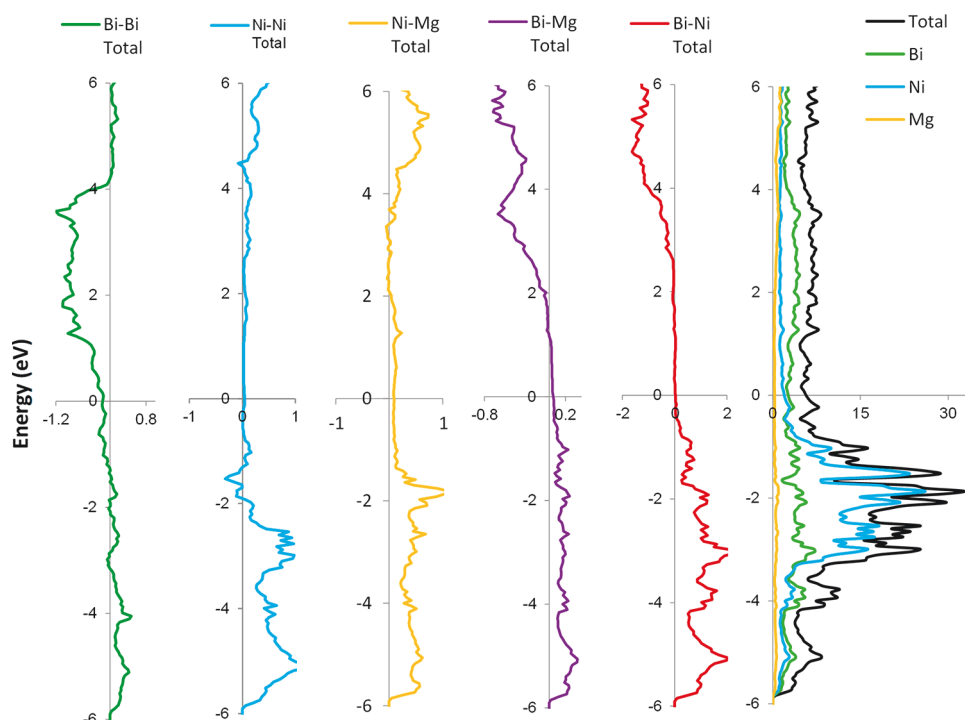
Figure 6. Total and partial density of states data calculated for $MgNi_2Bi_4$ (right), as energy vs density of states, and crystal orbital Hamilton population data calculated for specified bonds in the structure (left), as energy vs $-COHP$. E_f is defined as 0 eV.

The magnesium site in $MgNi_2Bi_4$ is located on a capping vertex of the bismuth-clad nickel chains, and it links these units into sheets that stack along the c-axis. The Mg−Ni bonds range from 2.563(8)−2.589(7) Å, which is shorter than those seen in Mg_2Ni (2.650−2.696 Å) and in MgNiBi (2.670 Å).[28,29] On the other hand, the Bi−Bi interactions between the 2-D sheets of $MgNi_2Bi_4$ appear to be elongated compared to those in the binary phases. These distances range from 3.387(2)−3.754(2) Å, which are noticeably longer than the corresponding distances in $NiBi_3$ and $NiBi_2$ of 3.486−3.675 Å and 3.118−3.323 Å, respectively.[16,25] This may indicate very weak interlayer bonding in $MgNi_2Bi_4$, leading to 2-D behavior. The anisotropy of the structure is reflected in the habit and behavior of the crystals—the axial directions were verified by face indexing, the long axis of the rod-shaped crystals is along the a-axis (the direction of the nickel zigzag chains), and the layers splay and shear along the ab-plane.

Magnetic Behavior and Resistance Studies. Because of its structural similarity to $NiBi_3$, the potential superconducting behavior of $MgNi_2Bi_4$ was investigated. No Meissner effect was observed in the magnetic susceptibility; instead, the sample was very weakly paramagnetic. The data in Figure 4 indicate that the sample demonstrates Pauli paramagnetic behavior with no localized or even itinerant moment on the nickel. The fit to a modified Curie−Weiss law ($\chi = [(C/T - \theta) + \chi_P]$, shown as dashed line in Figure 4) yields a negligible moment of 0.2 μ_B per nickel atom and a Weiss constant θ of −7.18(8) K, but the behavior is dominated by the Pauli paramagnetic term $\chi_P = 5.267(9) \times 10^{-4}$ emu/mol. The weak Curie−Weiss contribution and s-shape in the magnetization data is most likely due to the presence of a small amount of surface impurity, which often saturate at high fields. The slight anisotropy seen is attributed to the sample shape.

The temperature-dependent electrical resistivity data for electrical current applied along the a-axis are shown in Figure 5. Typical metallic behavior is observed, with a room temperature resistivity $\rho_{300\ K} \approx 42\ \mu\Omega$ cm and a residual low temperature resistivity $\rho_0 \approx 0.9\ \mu\Omega$ cm. These values indicate that the sample exhibits limited disorder scattering (i.e., a high crystalline quality), as evidenced by the residual resistivity ratio RRR = $\rho_{300\ K}/\rho_0$= 47. In agreement with the magnetic susceptibility data, there is no evidence for superconductivity over the measured temperature range, although a transition may occur at lower T.

Electronic Structure Calculations. Density of states (DOS) data shown in Figure 6 confirm the metallic nature of $MgNi_2Bi_4$, showing predominantly bismuth and nickel states present at the Fermi level. The nickel d-orbitals are concentrated in the −1 to −4 eV region below E_F; the bismuth states produce a broad band that ranges from −6 to +6 eV, and magnesium contributions are found largely above 4 eV. Crystal orbital Hamilton population (COHP) calculations show that Bi−Bi interactions are antibonding near E_F while Ni−Ni interactions are weakly bonding. These results correspond well with the same interactions in $NiBi_3$ as calculated by Ruck.[25] The Bi−Ni bonds exhibit optimal filling of bonding states and empty antibonding states and are likely the strongest bonding interactions that stabilize this compound. This is followed by the Mg−Bi and then Mg−Ni bonds. The Ni−Ni interactions appear to be essentially nonbonding at the Fermi level, while the Bi−Bi interactions are antibonding. The antibonding character of the Bi−Bi bonds suggests these layers are simply being held together by weak van der Waals forces, which is supported by how the crystals physically deform by splitting into thin sheets. These crystals remain as sheets rather than wires because of the stronger bonding character of the Ni−Mg interactions, which link the nickel chains together. The two-dimensional nature of the structure and bonding indicates this material may be amenable to exfoliation or intercalation chemistry. Similar

anisotropy of the electronic properties is indicated in the band structure (Figure S3), which shows large dispersion in the bands along the Z-T and Γ-S directions (in the *ab*-plane), and much less dispersion and therefore lower mobility along the S-R direction (along the *c*-axis).

CONCLUSION

$MgNi_2Bi_4$ grows readily from molten bismuth with a new structure type which shares a common building block with the structures of several Ni−Bi binary and ternary phases. $MgNi_2Bi_4$ does not appear to be superconducting, but further work is needed to determine if it can be doped into a superconducting state. The presence of $NiBi_3$ as a minor byproduct of the flux synthesis is also problematic; more investigations on the growth relationship between $MgNi_2Bi_4$ and $NiBi_3$ are needed. It is also notable that the known ternary phase space AE/T/Bi (AE = alkaline earth metals, T = Fe, Co, or Ni) is relatively empty; aside from the title compound, the MgNiBi half-Heusler alloy is the only other reported material.[29] Reactions in bismuth flux may enable the discovery of additional new phases.

Because of its sheet-like topography and two-dimensional structure, physical and chemical exfoliation of $MgNi_2Bi_4$ is being explored in order to determine how the properties of the layers vary from those of the bulk material. Physical exfoliation attempts have been unsuccessful thus far, as the separated slabs are significantly thicker than a monatomic layer. Chemical exfoliation was explored using sonication in several solvents including DMF and ethanol. While the formation of nano-particulates in solution was indicated by the observation of the Tyndall effect, TEM imaging of the dried solutions showed the particles to be largely amorphous. Further work on exfoliation using less aggressive methods is underway. We have also begun investigation of $MgNi_2Bi_4$ as a substrate for intercalation chemistry. However, exposure of crystals of this compound to iodine vapor resulted in degradation; reactions with other molecular species are being explored.

ASSOCIATED CONTENT

Ⓢⓘ Supporting Information
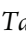
The Supporting Information is available free of charge at https://pubs.acs.org/doi/10.1021/acs.inorgchem.9b03196.

> Table of atomic positions and thermal parameters for $MgNi_2Bi_4$; powder X-ray diffraction data, SEM-EDS image, and band structure for $MgNi_2Bi_4$ (PDF)

Accession Codes

CCDC 1961839 contains the supplementary crystallographic data for this paper. These data can be obtained free of charge via www.ccdc.cam.ac.uk/data_request/cif, or by emailing data_request@ccdc.cam.ac.uk, or by contacting The Cambridge Crystallographic Data Centre, 12 Union Road, Cambridge CB2 1EZ, UK; fax: +44 1223 336033.

AUTHOR INFORMATION

Corresponding Author

Susan E. Latturner − *Florida State University, Tallahassee, Florida;* Ⓞ orcid.org/0000-0002-6146-5333; Email: slatturner@fsu.edu

Other Authors

Mary B. Hertz − *Florida State University, Tallahassee, Florida*

Ryan E. Baumbach − *Florida State University and National High Magnetic Field Laboratory, Tallahassee, Florida*

Complete contact information is available at:
https://pubs.acs.org/10.1021/acs.inorgchem.9b03196

Notes

The authors declare no competing financial interest.

REFERENCES

(1) Boehm, H. P.; Clauss, A.; Fischer, G. O.; Hofmann, U. Das Adsorptionsverhalten Sehr Dünner Kohlenstoff-Folien. *Z. Anorg. Allg. Chem.* **1962**, *316* (3−4), 119−127.

(2) Mas-Ballesté, R.; Gómez-Navarro, C.; Gómez-Herrero, J.; Zamora, F. 2D Materials: To Graphene and Beyond. *Nanoscale* **2011**, *3*, 20−30.

(3) Thygesen, K. S. Calculating Excitons, Plasmons, and Quasiparticles in 2D Materials and van Der Waals Heterostructures. *2D Mater.* **2017**, *4*, 022004.

(4) Saito, Y.; Nojima, T.; Iwasa, Y. Highly Crystalline 2D Superconductors. *Nat. Publ. Gr.* **2017**, *2*, 1.

(5) Morozov, S. V.; Novoselov, K. S.; Katsnelson, M. I.; Schedin, F.; Elias, D. C.; Jaszczak, J. A.; Geim, A. K. Giant Intrinsic Carrier Mobilities in Graphene and Its Bilayer. *Phys. Rev. Lett.* **2008**, *100* (1), 016602.

(6) Nicolosi, V.; Chhowalla, M.; Kanatzidis, M. G.; Strano, M. S.; Coleman, J. N. Liquid Exfoliation of Layered Materials. *Science* **2013**, *340* (6139), 1226419−1226419.

(7) Takano, Y.; Arai, N.; Arai, A.; Takahashi, Y.; Takase, K.; Sekizawa, K. Magnetic Properties and Specific Heat of MPS_3 (M = Mn, Fe, Zn). *J. Magn. Magn. Mater.* **2004**, *272−276*, E593.

(8) Kanamura, K.; Sakaebe, H.; Zhen, C.; Tokehara, Z. Solid-State Science and Technology: Application of Feoci Derivative for a Secondary Lithium Battery: I. Discharge and Charge Characteristics of Amorphous FeOOH Prepared by Ion Exchange Reaction of FeOCl Including Aniline. *J. Electrochem. Soc.* **1991**, *138* (10), 2971−2975.

(9) Granqvist, C. G. Electrochromic Tungsten Oxide Films: Review of Progress 1993−1998. *Sol. Energy Mater. Sol. Cells* **2000**, *60* (3), 201−262.

(10) Naguib, M.; Mashtalir, O.; Carle, J.; Presser, V.; Lu, J.; Hultman, L.; Gogotsi, Y.; Barsoum, M. W. Two-Dimensional Transition Metal Carbides. *ACS Nano* **2012**, *6* (2), 1322−1331.

(11) Kanatzidis, M. G.; Pöttgen, R.; Jeitschko, W. The Metal Flux: A Preparative Tool for the Exploration of Intermetallic Compounds. *Angew. Chem., Int. Ed.* **2005**, *44* (43), 6996−7023.

(12) Thompson, C. M.; Tan, X.; Kovnir, K.; Garlea, V. O.; Gippius, A. A.; Yaroslavtsev, A. A.; Menushenkov, A. P.; Chernikov, R. V.; Büttgen, N.; Krätschmer, W.; Zubavichus, Y. V.; Shatruk, M. Synthesis, Structures, and Magnetic Properties of Rare-Earth Cobalt Arsenides, RCo_2As_2 (R = La, Ce, Pr, Nd). *Chem. Mater.* **2014**, *26*, 3825−3837.

(13) Pfannenschmidt, U.; Rodewald, U. C.; Pöttgen, R. Bismuth Flux Crystal Growth of RERh$_6$P$_4$ (RE = Sc, Yb, Lu): New Phosphides with a Superstructure of the LiCo$_6$P$_4$ Type. *Monatsh. Chem.* **2011**, *142* (3), 219−224.

(14) Isaeva, A.; Rasche, B.; Ruck, M. Bismuth-Based Candidates for Topological Insulators: Chemistry beyond Bi$_2$Te$_3$. *Phys. Status Solidi RRL* **2013**, *7* (1−2), 39−49.

(15) Liu, Z. K.; Zhou, B.; Zhang, Y.; Wang, Z. J.; Weng, H. M.; Prabhakaran, D.; Mo, S. K.; Shen, Z. X.; Fang, Z.; Dai, X.; et al. Discovery of a Three-Dimensional Topological Dirac Semimetal, Na$_3$Bi. *Science* **2014**, *343* (6173), 864−867.

(16) Clarke, S. M.; Powderly, K. M.; Walsh, J. P. S.; Yu, T.; Wang, Y.; Meng, Y.; Jacobsen, S. D.; Freedman, D. E. Controlling Dimensionality in the Ni-Bi System with Pressure. *Chem. Mater.* **2019**, *31*, 955−959.

(17) Bruker. *SAINT*; Bruker AXS Inc.: Madison, Wisconsin, USA, 2012.

(18) Bruker. *SADABS*; Bruker AXS Inc.: Madison, Wisconsin, USA, 2001.

(19) Sheldrick, G. M. Crystal Structure Refinement with SHELXL. *Acta Crystallogr., Sect. C: Struct. Chem.* **2015**, *71*, 3−8.

(20) Jepsen, O.; Burkhardt, A.; Andersen, O. K. *The Program TB-LMTO-ASA*; Max-Planck-Institut für Festkörperforschung: Stuttgart, Germany, 2000.

(21) Dronskowski, R.; Blöchl, P. E. Crystal Orbital Hamilton Populations (COHP): Energy-Resolved Visualization of Chemical Bonding in Solids Based on Density-Functional Calculations. *J. Phys. Chem.* **1993**, *97*, 8617−8624.

(22) Skriver, H. L. *The LMTO Method: Muffin-Tin Orbitals and Electronic Structure* **1984**, 1.

(23) Andersen, O. K.; Jepsen, O. Explicit, First-Principles Tight-Binding Theory. *Phys. Rev. Lett.* **1984**, *53*, 2571−2574.

(24) Blavette, D.; Cadel, E.; Fraczkiewicz, A.; Menand, A. Three-Dimensional Atomic-Scale Imaging of Impurity Segregation to Line Defects. *Science* **1999**, *286* (5448), 2317−2319.

(25) Ruck, M.; Söhnel, T. Transmissionsoptimierte Einkristallstrukturbestimmung und elektronische Struktur von Bi3Ni / Transmission-Optimized Single-Crystal Structure Determination and Electronic Structure of Bi3Ni. *Z. Naturforsch., B: J. Chem. Sci.* **2006**, *61*, 785.

(26) Ruck, M. Bi$_{12}$Ni$_4$I$_3$: Ein Subiodid Der Intermetallischen Phase Bi$_3$Ni. *Z. Anorg. Allg. Chem.* **1997**, *623* (1−6), 243−249.

(27) Ruck, M. Bi$_{12,86}$Ni$_4$Br$_6$ Und Bi$_{12,86}$Ni$_4$I$_6$: Subhalogenide Mit Intermetallischen Und Salzartigen Schichtpaketen in Alternierender Abfolge. *Z. Anorg. Allg. Chem.* **1999**, *625* (3), 453−462.

(28) Schefer, J.; Fischer, P.; Hälg, W.; Stucki, F.; Schlapbach, L.; Didisheim, J.; Yvon, K.; Andresen, A. New Structure Results for Hydrides and Deuterides of the Hydrogen Storage Material Mg$_2$Ni. *J. Less-Common Met.* **1980**, *74* (1), 65−73.

(29) Nowotny, H.; Glatzl, B. Neue Vertreter Ternärer Verbindungen Mit C 1-Struktur. *Monatshefte für Chemie* **1952**, *83* (1), 237−241.